Bull Volcanol (2011) 73:1393–1406
DOI 10.1007/s00445-011-0476-x

RESEARCH ARTICLE

A spatter-forming, large-scale paroxysm at Stromboli Volcano (Aeolian Islands, Italy): insight into magma evolution and eruption dynamics

Sonia La Felice · Patrizia Landi

Received: 21 October 2010 / Accepted: 24 March 2011 / Published online: 1 June 2011
© Springer-Verlag 2011

Abstract This study focuses on a pyroclastic sequence related to a large-scale paroxysm that occurred during the seventeenth century AD and which can be considered one of the most powerful and hazardous explosive events at the volcano in the past few centuries. Paroxysms are energetic, short-lived explosions which sporadically interrupt normal Strombolian activity at Stromboli and commonly erupt a deep-derived, volatile-rich crystal-poor high-potassium basalt ("low porphyricity" (LP)), together with a shallow, degassed crystal-rich high-potassium to shoshonitic basalt ("high porphyricity" (HP)), which feed normal activity at the volcano. The studied deposit, crops out along the flanks of Sciara del Fuoco and, from base to top, consists of: (1) a layer of HP and LP ash and lapilli; (2) an unwelded layer of coarse HP lapilli and flattened dark scoriae; (3) weakly welded spatter made up of dense HP pyroclasts at the base, overlain by strongly vesicular LP clasts. The textural and chemical zoning of minerals and the glass chemistry of the LP products record repeated mafic recharge events, mixing with an old mushy body and episodes of rapid crystallization due to sudden degassing. Collapse of a foam layer originated by deep degassing probably triggered this large-scale, spatter-forming paroxysm. Decompression induced rapid degassing and vesiculation of the deep volatile-rich magma. The rapid ascent of the foamy magma blob pushed the shallow HP magma out and finally produced a fire fountain that emplaced the LP portion of the spatter.

Editorial responsibility: DB Dingwell

S. La Felice (✉) · P. Landi
Sezione di Pisa, Istituto Nazionale di Geofisica e Vulcanologia,
Via della Faggiola 32,
56126 Pisa, Italy
e-mail: lafelice@pi.ingv.it

Keywords Explosive paroxysm · Mineral zoning · Magma evolution · Eruption dynamics · Stromboli

Introduction

Stromboli volcano, the northernmost of the Aeolian Islands, is well known for its persistent activity, which started between the third and seventh centuries AD (Rosi et al. 2000). Normal Strombolian activity consists of continuous degassing and intermittent mild explosions from active vents located in the upper part (750 m a.s.l.) of Sciara del Fuoco, a horseshoe-shaped scarp formed through several flank collapses (Tibaldi 2001). At intervals of tens of minutes, jets of gas, incandescent magma fragments, ash and blocks are ejected several hundreds of metres upwards, mostly falling around the craters or rolling down the Sciara del Fuoco scarp. The maximum volume of solid fragments ejected during a Strombolian explosion is estimated to be ~7 m^3 (Ripepe et al. 2008). Outpouring lavas occasionally flow onto Sciara del Fuoco, with maximum volumes of the order of 10^6–10^7 m^3 (Marsella et al. 2008). Moreover, normal Strombolian activity is sporadically interrupted by more energetic, short-lived explosive eruptions of varying intensity and magnitude called "paroxysms" (Bertagnini et al. 2008 and references therein).

Normal activity and lava effusions are fed by a crystal-rich (~50 vol.%: plg ~ 65, cpx ~ 25, ol ~ 10), degassed high potassium to shoshonitic basalt (high porphyricity hereafter HP magma) which resides in the upper part of the plumbing system (Bertagnini et al. 2008 and references therein). During paroxysms a deeper crystal-poor (~10–12 vol.%: plg ~ 42–50, cpx ~ 47–30, ol ~ 11–20), volatile-rich basalt (low porphyricity hereafter LP magma) is erupted as highly vesicular gold-coloured pumices together with HP scoriae

(Bertagnini et al. 2008 and references therein). The HP magma derives from LP basalt mainly via crystallization driven by low-pressure water loss associated with a decrease in temperature from 1,140±15°C to 1,100±15°C (Métrich et al. 2001). Based on CO_2 and H_2O contents in melt inclusions, the deeper ponding zone is thought to be at a depth of 7–11 km (H_2O ~ 1.8–3.4 wt.%; CO_2 ~ 890–1,890 ppm) (Métrich et al. 2001, 2010; Bertagnini et al. 2003). The composition of plagioclase in equilibrium with the degassed HP magma (H_2O<0.6 wt.%; CO_2 <100 ppm according to Métrich et al. 2001; Landi et al. 2004; Di Carlo et al. 2006) suggests that the shallow magma storage is less than 900 m below the vents. A more recent study by Métrich et al. (2010) argues that CO_2 gas fluxing could enhance H_2O loss and crystallization of LP basalts: this would, therefore, deepen the roots of the shallow HP system to between 2 and 4 km below the vents. Sr isotope ratio studies (Francalanci et al. 2005) have inferred a crystal mush zone in an intermediate zone between the LP and HP reservoirs.

Paroxysms cover a wide range of intensities and magnitudes, making it difficult to apply a strict classification. The less energetic paroxysms (major explosions of Barberi et al. 1993) eject decimetre-sized ballistic blocks and bombs, lapilli and ash within a few hundred metres from the craters. On average, one to two "major explosions" have occurred per year over the past century (Barberi et al. 1993; Bertagnini et al. 1999). More powerful paroxysms are less frequent and consist of violent explosions accompanied by a detonation, during which scoriae and pumice bombs, metre-sized lithic blocks and ashes are ejected with mass discharge rates (10^5–10^6 kg s^{-1}) two or three orders of magnitude higher than those of typical Strombolian activity (Rosi et al. 2006). Ejecta can reach heights of several kilometres in the eruptive column and fall within several kilometres of the vents, affecting the two inhabited villages of the island. Only two events of this type have been observed in recent decades (5 April 2003 and 15 March 2007 explosions). Paroxysms that are even more energetic have occurred during persistent activity at Stromboli. They produced spatter deposits far from the vents at lower altitudes along the flanks of Sciara del Fuoco and can be considered the most hazardous activity of the volcano in the past millennium. According to recent paleomagnetic studies (Speranza et al. 2004, 2008), the "spatter-forming" large-scale paroxysms occurred in two time windows, during the twentieth century and between 1400 and 1600 AD. Archeomagnetic dating of spatter deposits by Arrighi et al. (2004) has also yielded an age of about 550±50 AD. Based on stratigraphic studies and components analysis, Bertagnini et al. (submitted, Bull Volcanol) identified two principal layers of spatter associated with two large-scale paroxysms. Comparison with paleomagnetic data (Speranza et al. 2004, 2008) led the authors to associate the upper deposit with the 1930 paroxysm and the lower one with paroxysms occurring at the turn of the seventeenth century. Rittmann (1931) provided a detailed report of the products erupted during the 1930 event; in particular, he described very fluid metre-sized clasts (cowpat-like) which covered the flanks of the volcano down to lower elevations (150–200 m a.s.l.).

This paper focuses on a spatter deposit cropping out on the N rim of Sciara del Fuoco, at an elevation of ~500 m a.s.l. and associated with the older "spatter-forming" event at the turn of seventeenth century. As production of LP pumice is a definite record of paroxysmal explosions, and the rise of deep LP magmas somehow governs this type of explosive activity, this study mainly deals with LP products. Whole-rock chemical analysis, textural study and microprobe analysis of minerals and glasses were carried out to shed light on the nature of these specific products and to assess correlations between petrochemistry and eruptive dynamics.

Spatter deposits and sampling

The studied samples were mainly collected along the northern rim of Sciara del Fuoco in a stratigraphic section 520 m a.s.l. and 800 m from the present craters (GPS lat 518821; lon 4294902), where almost continuous deposits of agglutinated spatter crop out. The stratigraphic sequence lies above a substrate consisting of yellowish, partially reworked ash beds. Three layers can be distinguished from the base upward (Fig. 1):

Layer 1 <5 cm thick basal layer of fine to coarse ashes and lapilli consisting of glassy shiny black scoriae, golden pumice and lithic fragments

Layer 2 <15 cm layer of coarse lapilli and intensely flattened, dark crystal-rich scoria bombs (Fig. 1a)

Layer 3 Spatter deposit *s.s.* with a maximum thickness of ~50 cm consisting of two parts differing in texture and crystal content: (1) a <10-cm thick basal layer made up of dense, poorly vesicular crystal-rich clasts (Fig. 1b) with virtually obliterated outlines; (2) weakly agglutinated, dark pyroclasts in which clast outlines are partly retained. The pyroclasts are flattened and have brown highly vesicular (sponge-like), LP core (Fig. 1c) and golden chilled outer margins (Fig. 1d). They include fragments (mostly <1-2 cm) of crystal-rich (HP) scoriae (Fig. 1e) and dispersed millimetre-sized crystals. Reddish sub-planar lenses of loose crystals, mostly clinopyroxenes, mark the contacts where pyroclasts stuck together upon impact (Fig. 1f).

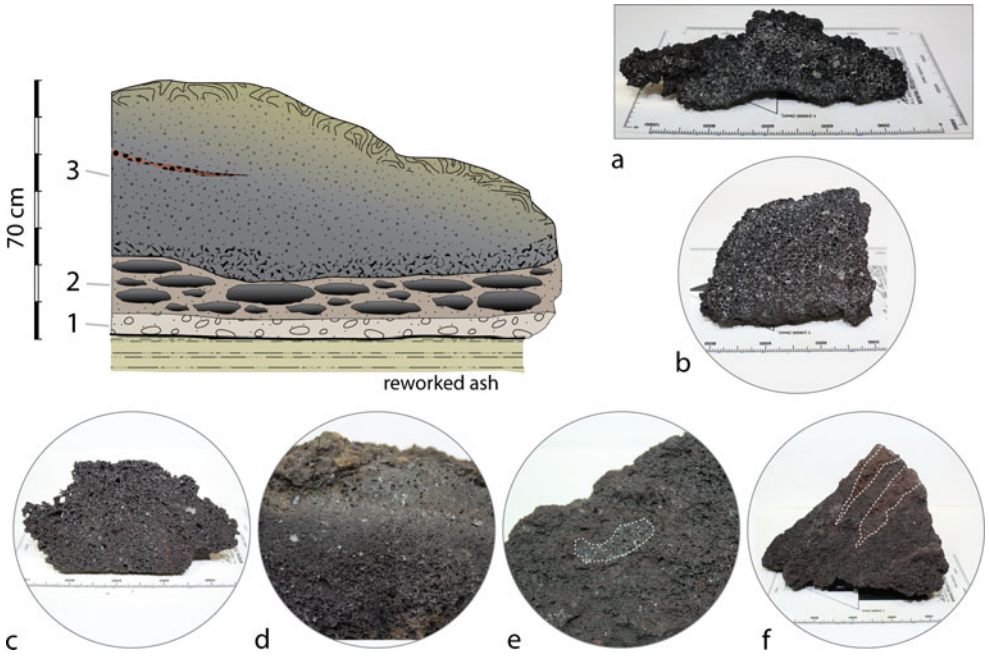

Fig. 1 Representative sketch of the pyroclastic sequence of the seventeenth century AD paroxysm. Outcrop at about 520 m a.s.l. on the northern flank of Sciara del Fuoco. From base to top three layers can be distinguished: *1* fine to coarse ash and lapilli; *2* coarse lapilli and decimetre-sized flattened dark crystal-rich scoriae (*a*); *3* weakly agglutinated spatter made up of a basal portion consisting of dense HP clasts (*b*) overlain by LP pyroclasts with brown, highly vesicular (sponge-like) core (*c*) and golden-coloured chilled margins (*d*). They include crystal-rich fragments (*e*) and reddish crystal-enriched sub-planar lenses (*f*)

Seven samples were collected from the base to the top of the sequence (layer 1: PST12; layer 2: ST561, ST566; layer 3: PST11, ST560, ST563, ST567). Based on the stratigraphic study of Bertagnini et al. (submitted, Bull Volcanol), we also selected samples for petrochemical analysis from three different localities correlated with the same eruptive event: the NE flank of Sciara del Fuoco at 550 m a.s.l. (layer 1: ST514; layer 3: ST515, ST531); the NE flank of Sciara del Fuoco at 400–430 m a.s.l. (layer 1 ST538; layer 3: ST536) and the SW flank of Sciara del Fuoco at 680 m a.s.l. (layer 1: ST546).

Analytical methods

Whole-rock chemical analyses, textural studies and microprobe analyses of mineral phases and glasses were performed on selected samples.

Modal analyses of minerals>100 μm in size were performed on HP samples using an optical microscope equipped with a point counter; ~1,200 points, excluding vesicles, were counted in each sample. Measurements of the density of clasts were performed following the method suggested by Houghton and Wilson (1989) to calculate sample vesicularity using a dense rock equivalent value of 2,800 kg m^{-3} (Pistolesi et al. 2008).

Whole-rock major and trace elements were analyzed using ICP–MS and ICP–AES at Activation Laboratories Ltd (Ontario, Canada) in accordance with the 4LITHORES protocol. Pyroxene, plagioclase and olivine crystals were hand-picked from crushed and sieved clasts, mounted in epoxy resin, sectioned and polished. Chemical analyses of minerals and glasses were performed using a *JEOL JXA-8200* electron microprobe equipped with a WD/ED combined system (15 kV voltage, a 5-μm beam spot and 5 nA beam current) at Istituto Nazionale di Geofisica e Vulcanologia in Rome. The texture of minerals and glasses and additional chemical analyses were performed with a LEO-1430 scanning electron microscope equipped with an Oxford EDS microanalytical system at INGV in Catania and with a Philips XL30 scanning electron microscope equipped with an EDAX DX4 microanalytical system at DST, University of Pisa.

Texture and mineral chemistry

Crystal-rich and crystal-poor products collected from the base to the top of the pyroclastic sequence have whole rock compositions (Table 1) similar to those of the HP and LP products erupted in the past century, i.e. in the range between shoshonitic basalts and HK basalts (Bertagnini et al. 2008 and references therein).

HP products

The dark flattened scoriae below the spatter (layer 2, samples ST561, ST566) and the basal crystal-rich portions of the spatter deposit (layer 3, samples ST560, ST567) show the same textural and mineralogical features as those

Table 1 Major (wt.%) and trace (ppm) element bulk rocks of selected samples

	PST11n HP-Layer 3	ST560b HP-Layer 3	ST560c LP-Layer 3	ST561 HP-Layer 2
Wt.%				
SiO_2	51.05	51.03	51.30	51.01
Al_2O_3	16.74	17.25	15.72	17.00
Fe_2O_3T	8.28	8.51	8.35	8.57
MnO	0.15	0.15	0.15	0.15
MgO	6.15	6.29	7.29	6.26
CaO	11.02	11.18	11.89	11.03
Na_2O	2.49	2.60	2.42	2.54
K_2O	2.18	2.14	1.95	2.08
TiO_2	0.82	0.90	0.79	0.85
P_2O_5	0.51	0.54	0.47	0.50
LOI	0.24	−0.20	−0.02	−0.17
Total	99.63	100.39	100.31	99.82
ppm				
Sc	31	33	36	31
Be	2	2	2	2
V	267	281	272	279
Cr	100	80	180	90
Co	29	27	31	30
Ni	50	40	60	50
Cu	120	90	130	100
Zn	80	60	70	80
Ga	15	15	14	15
Rb	67	65	57	64
Sr	704	739	679	688
Y	23.9	23.1	23.3	24.6
Zr	170	164	155	166
Nb	23	24.7	21.9	23.8
Cs	4.6	4.8	3.8	4.4
Ba	1023	955	928	961
La	48.2	41.9	44.6	47.1
Ce	91.9	82.1	85.6	89.5
Pr	11.4	10.4	10.7	11.1
Nd	41.3	39.6	40	40.6
Sm	7.88	7.62	7.69	7.96
Eu	1.96	1.9	1.9	1.93
Gd	6.47	6.1	6.23	6.44
Tb	0.87	0.87	0.87	0.9
Dy	4.66	4.65	4.52	4.8
Ho	0.85	0.86	0.83	0.88
Er	2.29	2.31	2.26	2.41
Tm	0.321	0.333	0.316	0.348
Yb	2.13	2.24	2.09	2.32
Lu	0.316	0.341	0.317	0.349
Hf	3.3	3.3	3.2	3.2
Ta	1.24	1.52	1.14	1.23
Pb	18	17	16	17
Th	15.1	15.1	13.5	14.6
U	4.2	4.35	3.77	4.08

Analytical error on each element contents can be estimated by last significant digits/decimal places; all iron calculated as Fe_2O_3

LOI loss on ignition

of the HP scores and lavas emitted from Stromboli in the past century (Landi et al. 2004, 2006; Francalanci et al. 2004). They have a porphyritic texture with a 45–52 vol.% crystals of zoned plagioclase An60–88 (26–32 vol.%), zoned clinopyroxene Fs5–17 (12–17 vol.%), and olivine Fo70–73 (5–6 vol.%) set in a hypocrystalline to glassy shoshonitic groundmass. Euhedral rims <20 μm wide in textural equilibrium with the groundmass have a nearly constant composition, i.e. plagioclase An62–68, clinopyroxene Fs13–14 and olivine Fo71–73.

LP products

Much of the spatter is made up of highly vesicular sponge-like clasts. Vesicularity was measured in a selected sponge-like sample (ST563) about 40 cm in diameter. Nineteen sub-samples, including portions of the inner portion and quenched outer margin, yielded a vesicularity of 74 vol.% (SD=3.4). Pyroclasts display a population of <100 μm to millimetre-sized vesicles uniformly distributed throughout the sample. The smaller bubbles (<100 μm) have spherical to subspherical shapes and are found in the septa between larger bubbles and in the quenched glass of the outer margins of clasts (Fig. 2a). The larger vesicles, ellipsoidal to amoeboidal, are the coalesced products of two or more smaller vesicles (Fig. 2b). In the innermost part of the clast, the virtually holocrystalline groundmass is a mosaic of skeletal crystals of plagioclase (~100–150 μm), pyroxene and olivine which locally form radiating textures (Fig. 2d). Towards the external part, the groundmass is cryptocrystalline and contains sparse, ~100–150 μm long microlites of plagioclase with a skeletal texture (Fig. 2c). Only the outer margins have a glassy groundmass with rare microlites of skeletal plagioclase <50 μm. These textural changes reflect an increase in the heat-loss rate from core to rim of the sponge-like pyroclasts, suggesting that they were produced from a microlite-free, volatile-rich LP magma and that crystallization of the interior groundmass occurred during slow post-depositional cooling.

Two samples of sponge-like products (ST560, ST563) have been selected for the textural and chemical study of minerals. The sponge-like pyroclasts yield ~20–25 vol.% crystals of clinopyroxene, the most abundant mineral phase (~60–70% of the total crystals), olivine and plagioclase with chemical and textural characteristics similar to those of the LP products erupted during intermediate- to large-scale paroxysms (Métrich et al. 2001, 2005, 2010; Bertagnini et al. 2003; Francalanci et al. 2004).

On the whole, clinopyroxenes are euhedral crystals with zoned compositions ranging from Mg# [molar 100 × Mg/(Mg+Fe^{2+})] 71 to 92, Wo38–48 and Fs5–17 (Table 2). Zoning within single crystals can be complex, including patchy, reverse or step zoning with growth bands of

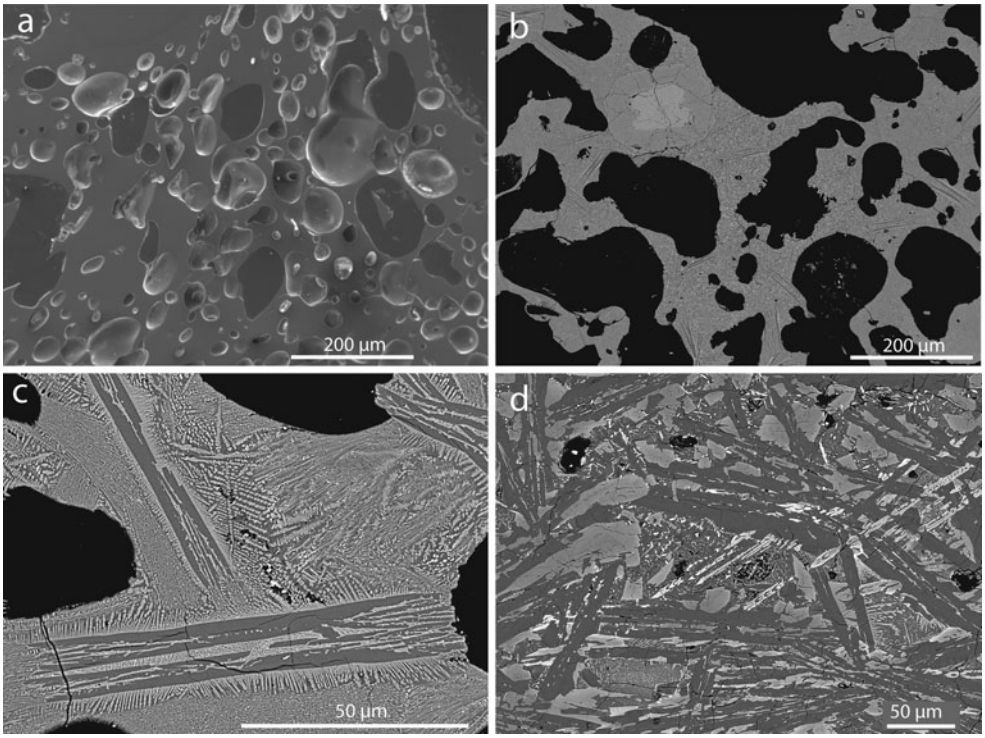

Fig. 2 SEM images of the groundmass of the spatter clasts. **a** Chilled outer margins characterized by glassy groundmass with abundant small (mostly <100 μm) spherical or elongated bubbles; **b** crystalline groundmass in the inner portions with large irregularly shaped and coalesced bubbles and cpx phenocryst (*upper left*); **c** cryptocrystalline groundmass of the inner margins with skeletal plagioclase overgrown by thin pyroxenes; **d** holocrystalline texture in the core, crowded with skeletal crystals of plagioclase (*dark grey*) and olivine (*white*) with intergranular pyroxene (*light grey*). **a** SE image; **b**–**d** BSE images

variable thickness. Based on the texture and composition of the core, two main clinopyroxene populations have been identified (Fig. 3): (1) crystals with a homogeneous Fe-rich resorbed core Mg# 71–75 (Fs15–17, Wo41–44) that in some cases has abundant magnetite inclusions. Dissolution surfaces are highlighted by rounded or rough shapes with deep channels along the main crystollagraphic growth axis of the crystal (Fig. 3a); (2) crystals showing patchy zoned cores (Fig. 3b–d), with less and more iron-rich portions characterized by Mg# 83–88 (Fs6–9) and Mg# 77–83 (Fs10–13), respectively, and a spongy cellular texture due to abundant voids, sometimes rimmed by glass, and vesicular, irregular-shaped melt inclusions. Strongly corroded, Fe-rich zones with Fs15–17 (Mg# 71–75) are common (Fig. 3b, d). Interestingly, olivine Fo83–86 is sometimes included in the spongy cores (Fig. 4b, c). Both types of crystals are surrounded by euhedral mantles of variable width ranging from 50 to 500 μm (Fig. 3e, f). Mantles can be (1) homogeneous in composition Fs7–Fs8 (Mg# 87–85), (2) normally zoned from Fs5 to Fs7 (Mg#91 to 87) or (3) step-zoned with bands ranging in composition from Fs6 to Fs10 (Mg# 89–82), sometimes with Fe-rich thin layers Fs13–14 (Mg# 78–75) growing on dissolution surfaces. The composition of the outermost band is mainly Fs7–Fs8 (Mg# 87–85). Crystals of the HP magma wetted by LP glass with thin rims (<10 mm) Fs7–10 probably entered the LP magma during syn-eruptive mingling.

There are three main olivine populations (Fig. 4a–c): (1) patchy zoned Fo82–86, spongy crystals with lobate margins, crowded with irregular amoeboid-shaped melt inclusions and empty bubbles (Fig. 4a); (2) euhedral Mg-rich crystals displaying reverse zoning with a homogeneous core Fo82 and an outer zone Fo88–90, sometimes with outermost rims <10 μm Fo83 (Fig. 4b). Reverse zoned crystals with core Fo72, intermediate zone Fo75–76 surrounded by a corona Fo87–88 are sporadic; (3) crystals with a Fe-rich, strongly resorbed core (Fo70) surrounded by a zone crowded with melt inclusions and empty gas bubbles, Fo~76–80 up to Fo83 in the outermost rim (Fig. 4c). According to Métrich et al. (2001), the latter are regarded as crystals inherited from an HP magma which experienced dissolution events and rapid crystallization during magma ascent.

Plagioclase crystals mostly show cores with complex zoning inherited from the HP magma, mantled by a bytownitic (~An85) skeletal to sieve-textured corona <50–100 μm (Fig. 4d, e) likely grown during the ascent and rapid degassing of the magma (Landi et al. 2004). Crystals with skeletal texture of bytownitic composition are less common (Fig. 4f). Plagioclase does not crystallize in the volatile-rich LP magma before degassing (Di Carlo et al. 2006).

Note that a large number of the phenocrysts from the sponge-like LP clasts are inherited from the HP magma; they are either euhedral usually wetted by brown shoshonitic glass or surrounded by reaction rims. This observation indicates extensive syn-eruptive mingling between HP and LP magmas, which is specific to pumice erupted during paroxysms.

Table 2 Representative analyses of clinopyroxene in LP clasts from the spatter

Sample	ST560									
Crystal	px 17	px 12	px 12	px 12	px15	px 9	px19	px15	px 8	px18
Type	Fe-rich	Patchy	Patchy	Patchy	Fe-rich	Patchy	Fe-rich	Fe-rich	Patchy	patchy
Position	Core	Remn	Light p.	Dark p.	Mantle	Mantle	Rim	Rim	Rim	Rim
SiO_2 wt.%	50.96	51.47	52.39	51.97	51.52	53.22	51.72	52.31	51.52	52.30
TiO_2	0.93	0.69	0.62	0.34	0.59	0.25	0.33	0.43	0.41	0.44
Al_2O_3	3.42	2.52	2.15	3.26	3.41	1.72	3.67	3.07	3.40	3.57
FeO	9.88	9.12	7.31	4.44	6.73	2.93	4.96	4.46	3.63	4.72
MnO	0.28	0.30	0.21	0.12	0.20	0.08	0.12	0.08	0.12	0.11
MgO	14.84	14.65	15.84	16.03	15.57	17.49	15.58	16.63	16.65	16.39
CaO	19.82	20.58	21.43	22.73	21.89	22.67	22.80	22.12	22.42	22.35
Na_2O	0.38	0.31	0.20	0.21	0.28	0.17	0.20	0.15	0.16	0.18
Cr_2O_3	0.05	0.01	0.00	0.05	0.01	0.54	0.05	0.23	0.69	0.18
TOT	100.57	99.65	100.14	99.14	100.21	99.06	99.43	99.47	98.99	100.24
Wo mol%	40.95	42.59	43.43	46.78	44.70	45.93	47.06	45.33	46.22	45.67
En	42.67	42.19	44.67	45.90	44.24	49.31	44.76	47.43	47.76	46.62
Fs	16.39	15.22	11.90	7.32	11.05	4.76	8.18	7.25	6.03	7.71
Mg#	72.8	74.1	79.4	86.6	80.5	91.4	84.8	86.9	89.1	86.1
Al/Ti mol	5.7	5.8	5.5	14.1	9.3	10.6	17.7	11.1	13.4	12.8

Total iron as FeO, Mg#=molar $100\times Mg/(Mg+Fe^{2+})$

Remn Fe-rich remnant of the core, *p.* patches, *type* mineral type, *Patchy* patchy-zoned core type, *Fe-rich* Fe-rich core type, *Wo* wollastonite, *En* enstatite, *Fs* ferrosilite

Glass composition

Four samples from the base of the sequence (ST514, ST538, ST546, PST12), one flattened scoria (ST566) and five sponge-like clasts from the upper part of the spatter (ST515, ST531, ST536, ST560, ST563) were selected for the chemical analysis of glassy matrices. Only the microlite-free, glassy matrix of the quenched outer margins of the sponge-like clasts was analyzed (Table 3)

The glassy matrix of the HP scoriae and ash and lapilli at the base of the pyroclastic sequence have nearly constant, shoshonitic compositions (MgO 3.3–3.9 wt.%, K_2O 3.9–4.6 wt.% and CaO/Al_2O_3 0.45–0.50) pertaining to the HP products erupted during persistent activity at Stromboli (Fig. 5). From the base to the top of the sequence, the glassy matrices of the LP products cover a relatively large compositional interval in the field of shoshonitic basalts (MgO 5.2–6.1, K_2O 1.9–3 and CaO/Al_2O_3 0.52–0.64). Note that the matrices of the LP pumice from the basal layer are slightly more evolved than those of the LP clasts from the uppermost spatter. The less evolved glass (average composition MgO 5.67±0.20 wt.%, K_2O 2.36±0.10 wt.%) and the more evolved one (average composition MgO 5.35±0.15 wt.%, K_2O 2.72±0.10 wt.%) form two distinct clusters, with the limit at MgO ~5.5 wt.% and K_2O 2.5 wt.%, with no apparent compositional gap.

Discussion

The petrochemical characteristics of products emitted during the spatter-forming paroxysm at the turn of the seventeenth century highlight a base to top compositional zoning due to (1) the emission of HP magma and of minor quantities of relatively evolved LP magma at the beginning of the event (basal ash and lapilli fallout); (2) the emission of HP magma forming a layer of flattened scoriae and evolving into welded spatter (base of the spatter deposit), followed by (3) the emission of a large quantity of LP magma resulting in the emplacement of weakly agglutinated spatter (intermediate portion and top of the spatter deposit).

Both HP and LP products, as a whole, show the same bulk composition, mineral chemistry and crystal zoning as the HP and LP magmas erupted from Stromboli since the beginning of the persistent activity at the volcano. Study of the glassy matrix reveals a systematic compositional zoning of LP products along the sequence, highlighting the chemical zoning of the LP reservoir. Although LP magmas with different chemistry and/or degree of evolution have been observed in the past (Métrich et al. 2001) as both erupted products and MI hosted in minerals, the zoning is here clearly observed for the first time from the base to the top of a single eruptive sequence.

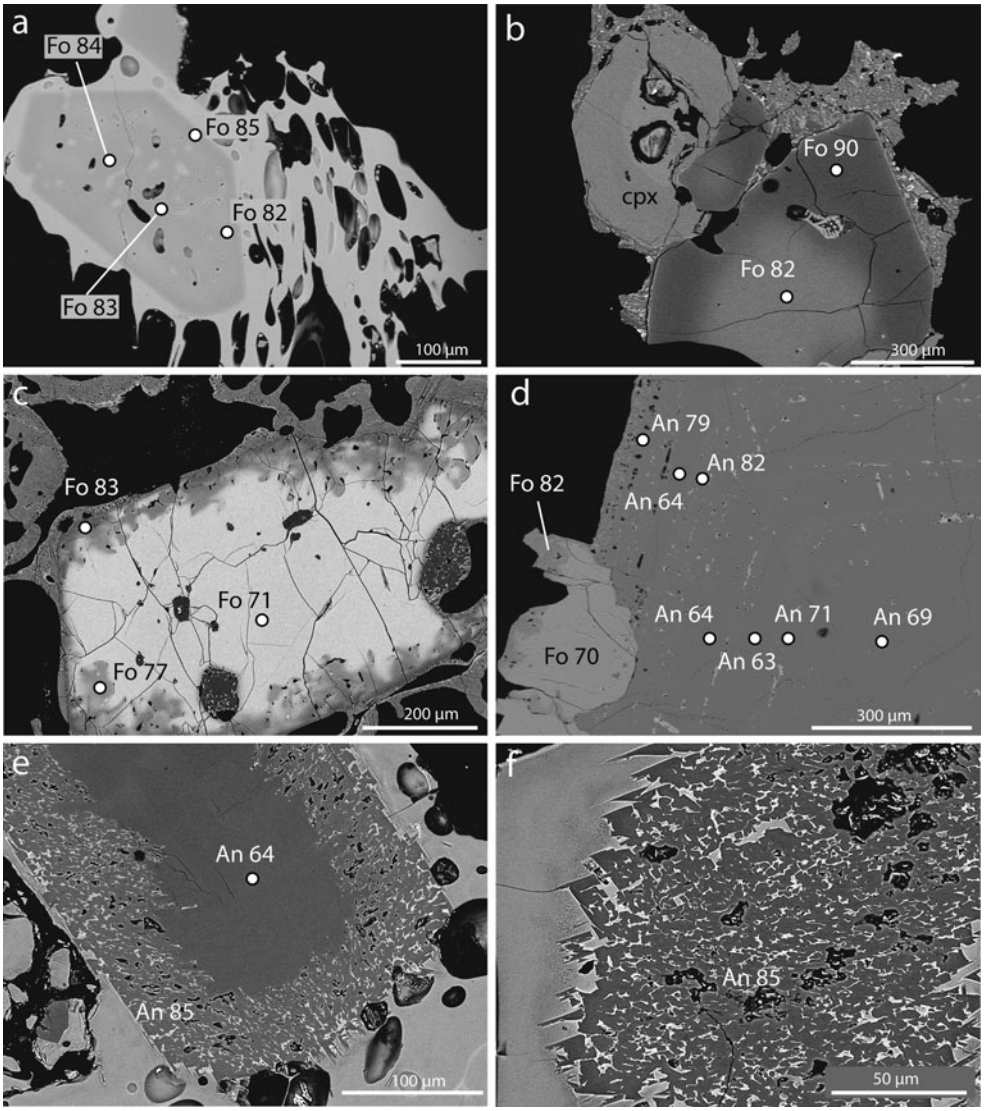

Fig. 3 BSE images of clinopyroxene phenocrysts from the LP clasts. **a** Crystal with deeply resorbed Fe-rich (Mg#74) core, with abundant magnetite inclusions, surrounded by homogeneous mantle Mg#85; **b** crystal with patchy zoned, spongy cellular core, including strongly corroded Fe-rich remnants and surrounded by step-zoned mantle; **c** patchy-zoned, spongy cellular core mantled by normal zoned, mafic rim Mg#89–91. Inclusion of olivine~Fo85 are common in the patchy zoned, spongy cellular cores; **d** particular of patchy zoned, spongy cellular core showing vesicular glass inclusions; **e**, **f** particular of step zoned mantle. *Black and white numbers* indicate Mg# [molar $100\times Mg/(Mg+Fe^{2+})$] and Fs mol.%, respectively

Evolution of LP glasses

Using least-squares mass balance calculations, the most evolved glass can be obtained from the less evolved one by fractionation of 4–5 wt.% crystals of clinopyroxene. The behaviour of Al_2O_3 and alkali, which maintain constant values from the less to the more evolved glasses (Fig. 5), rules out the involvement of plagioclase and suggests that the evolution process occurred in a volatile-rich magma with $H_2O>2$ wt.% (Di Carlo et al. 2006). Systematic studies of melt inclusions hosted in olivine from the LP magma found relatively high water contents of between 1.8 and 3.4 wt.% in the magmas erupted during the paroxysms and, based on CO_2–H_2O equilibrium, constrained the pressure of LP reservoirs to between 250 and 190 Mpa (Métrich et al. 2010). MELTS computations (Ghiorso and Sack 1995) predict that at these conditions clinopyroxene is the liquidus phase in a melt with the composition of the less evolved glass at NNO+0.5 redox conditions (as suggested by Pichavant et al. 2009). Olivine is the liquidus phase only at lower pressures and high water contents (P 150 MPa, H_2O 3.5 wt.%). Clinopyroxene remains the main phase crystallizing in the 1130–1115°C temperature range (0.3 wt.% ol, 1.5 wt.% cpx). MELTS computations confirm that the evolution of the LP melt is mainly controlled by crystallization of clinopyroxene, with minor involvement of olivine. In the following we speculate on the origin of the different types of clinopyroxene and compare the texture and composition of clinopyroxene with those of olivine. Olivine basically presents the same characteristics and variety found in the pumice of other paroxysms and described in detail in previous works (Métrich et al. 2001, 2005, 2010; Bertagnini et al. 2003). Conversely, textural and chemical characteristics of clinopyroxene in LP pumice until now have not been studied exhaustively.

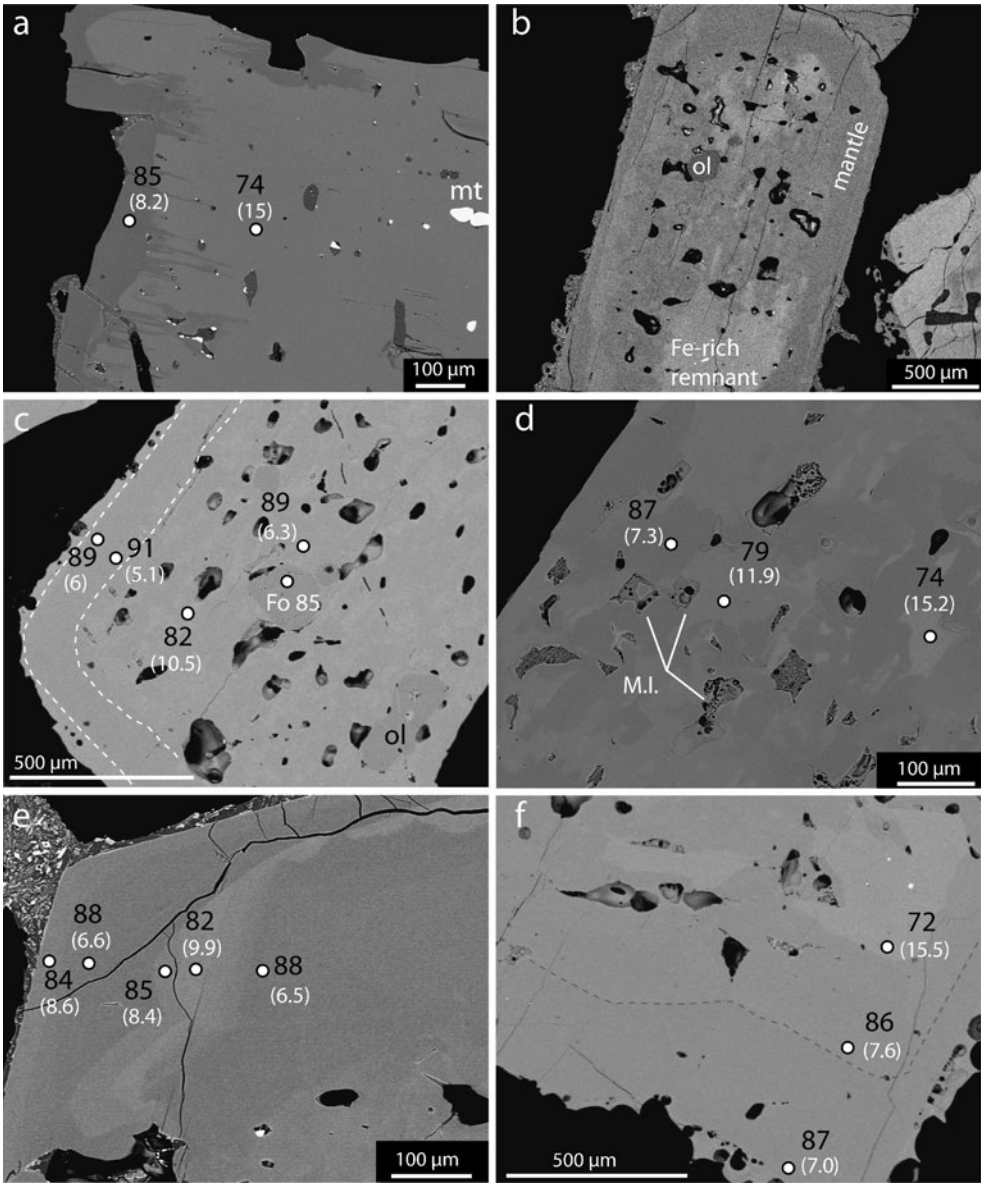

Fig. 4 BSE images of olivine and plagioclase crystals. **a** Patchy-zoned spongy olivine, crowded with irregular ameboid-shaped melt inclusions, empty bubbles and lobate margins; **b** reverse-zoned, euhedral Mg-rich olivine; **c** olivine with resorbed Fe-rich core, surrounded by a Mg-rich zone crowded with melt inclusions and voids; **d** oscillatory zoned plagioclase inherited from shallow HP magma, mantled by a thin sieve textured, bytownitic corona. Adjacent olivine shows Mg-rich rims; **e** plagioclase inherited from shallow HP magma mantled by a bytownitic, skeletal to sieve textured corona; **f** skeletal plagioclase with bytownitic composition

Origin of clinopyroxene and inferences on magma evolution

Three crystallization environments can be distinguished in the Mg# vs Al_2O_3 wt.% plot (Fig. 6). The high-Mg# group crystallized from the poorly evolved LP magmas or more primitive melts, whereas pyroxene ~ Mg# 75–78 (~Fs12–14) crystallized in a second environment from the shoshonitic melts of the HP magmas, as discussed below. Different Mg# over the same Al_2O_3 wt.% range reflect the extensive crystallization of plagioclase in HP magmas. A third environment is mainly delineated by the Fe-rich resorbed cores with lower Mg# (Fs15–17, Mg# 71–75). These pyroxenes are too evolved to have crystallized in the HP environment. They are considered xenocrysts possibly derived from an old crystal mush, uncorrelated with the present magma system of Stromboli (Francalanci et al. 2005) and periodically disrupted and sampled by the LP magmas.

Cellular textured, patchy-zoned crystals can develop through a variety of processes, including melt-crystal re-equilibration (when the crystal enters melts with which it is not in equilibrium) or rapid crystal growth and the formation of a quenched texture (Streck 2008 and references therein). In the case of the pyroxene of the LP products, it is difficult to determine whether its texture and zoning are due to dissolution or rapid growth. Remnants of Fe-rich pyroxene included in the patchy zoned, cellular areas (Fig. 3b) suggest melt-crystal re-equilibration of a crystal not in equilibrium with the LP magma. Other evidence, such as its boxy appearance and abundant inclusions of vesicular

Table 3 Average compositions of glasses from selected samples

	Layer 1				Layer 2	Layer 3			
Sample	PST12	PST12	ST514	ST514	ST566	ST563	ST560	ST515	ST536
No. of analysis	(13)	(16)	(25)	(25)	(17)	(20)	(38)	(18)	(15)
	LP	HP	LP	HP	HP	LP	LP	LP	LP
SiO_2 wt.%	50.32	52.24	51.29	53.19	53.21	50.31	50.90	50.86	49.78
TiO_2	0.94	1.47	0.93	1.51	1.49	0.88	0.86	0.85	0.85
Al_2O_3	17.80	15.51	17.88	15.43	15.27	17.63	17.95	17.46	17.27
FeO	7.55	9.59	7.68	9.75	9.54	7.51	7.68	7.40	7.30
MnO	0.14	0.18	0.15	0.19	0.20	0.15	0.14	0.15	0.15
MgO	5.34	3.61	5.37	3.59	3.65	5.74	5.71	5.92	5.76
CaO	9.86	7.30	10.08	7.42	7.42	10.62	10.84	10.86	10.50
Na_2O	2.99	3.38	3.07	3.42	3.33	2.77	2.73	2.80	2.71
K_2O	2.82	4.23	2.72	4.08	4.44	2.51	2.33	2.43	2.30
P_2O_5	0.57	0.99	0.56	0.97	0.99	0.51	0.50	0.57	0.50
Cl	0.14	0.13	0.13	0.12	0.12	0.12	0.13	0.14	0.13
BaO	0.13	0.21	0.16	0.20	0.18	0.13	0.14	0.09	0.11
Total	98.58	98.81	99.98	99.84	99.81	98.83	99.90	99.51	97.34
CaO/Al_2O_3	0.55	0.47	0.56	0.48	0.49	0.60	0.60	0.62	0.61
FeO/MgO	1.41	2.66	1.43	2.72	2.61	1.31	1.35	1.25	1.27

LP crystal-poor products, *HP* crystal-rich products

glass and voids rimmed by glass, point to rapid growth under degassing conditions. Olivine inclusions whose compositions are in equilibrium with LP melts (Fo83–86) provide further evidence that the cellular textured, patchy zoned cores grew in the LP magma. We suggest that the cellular textured, patchy zoned cores originated through dissolution of Fe-rich crystals coincident with crystallization of Mg-rich pyroxene (Umino and Horio 1998) during ascent and degassing of the LP magma. The crystallization conditions were likely the same as those of olivine Fo82–86, which bears a high density of irregular melt inclusions and bubbles that Bertagnini et al. (2003) ascribed to rapid growth during LP magma ascent and degassing.

The texture and composition of mantles around the pyroxene crystals indicate that the different cores shared a late growth history during which they experienced crystallization and dissolution events in melts with different degrees of evolution. A positive correlation between Mg# and Cr_2O_3 wt.% or Al_{tot}/Ti molar ratio (Fig. 7) confirms that differences in the chemistry of pyroxene are not due to intracrystalline diffusion but reflect magmatic compositions.

To constrain the compositions of liquids in equilibrium with the different clinopyroxene compositions, the XFe*/XMg ratio (with Fe*=Fe^{2+} as total iron) was calculated for Kd_{Fe-Mg} cpx/liq $\left[\text{defined as } \left(X\text{Fe}_{cpx}/X\text{Mg}_{cpx}\right)/\left(X\text{Fe}_{liq}/X\text{Mg}_{liq}\right), \text{considering all iron as } Fe^{2+}\right]$ ranging from 0.22 to 0.24, as suggested by experimental studies on shoshonitic products from Stromboli (Conte et al. 2006) (Fig. 8). Pyroxene Mg# 74–76 (~Fs14) is in equilibrium with the shoshonitic HP matrices, whereas compositions of glass in equilibrium with Fe-rich pyroxene Mg#71–75 were not found. Only pyroxene ~ Mg# 84–86 (Fs7–8), found in homogeneous mantles and in the rims of the step-zoned ones, is in equilibrium with liquids having the same composition as the glassy matrices. The less evolved compositions (Fs 4–5, Mg# 90–92) commonly found in the innermost part of the mantle are in equilibrium with more primitive melts (XFe/XMg ~ 0.5) never erupted from Stromboli and only found as MI in olivine Fo88–91 (Métrich et al. 2001; Bertagnini et al. 2003). We ascribe the normal-zoned mantles Fs5–7 to mixing with more primitive melts, which induced early crystallization of Mg-rich pyroxene followed by crystallization of more evolved pyroxene in equilibrium with the residing LP melts. Mixing with primitive melts also induced crystallization of Mg-rich olivine (Fo89–90), as suggested in previous studies (Bertagnini et al. 2003). The step-zoned mantles between Fs6 and Fs10 (Mg# 89–82) represent repetitive episodes of growth and dissolution due to refilling and crystallization in equilibrium with variably evolved LP melts (Fig. 8).

Preliminary conclusions

Based on mineral textures and crystal-liquid equilibria we conclude that pyroxene in the LP magma mainly grew on xenocrysts incorporated into the magma during its ascent

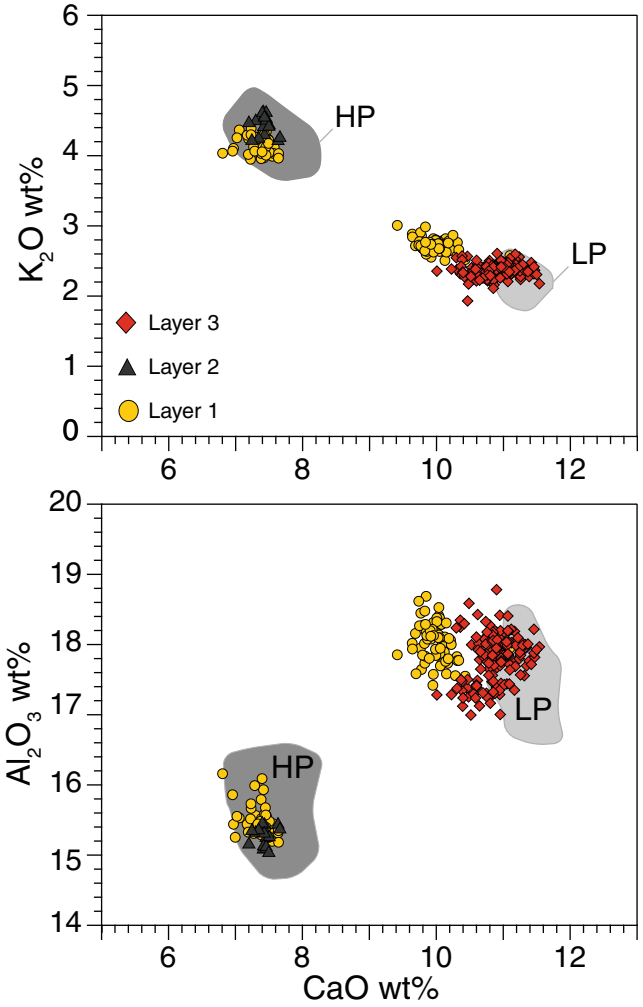

Fig. 5 Composition of the glassy matrices plotted in CaO versus K_2O and CaO versus Al_2O_3 diagrams. The *shadow areas* represent the compositional fields of the matrices of HP (*dark grey*) and LP (*light grey*) products erupted in the past years

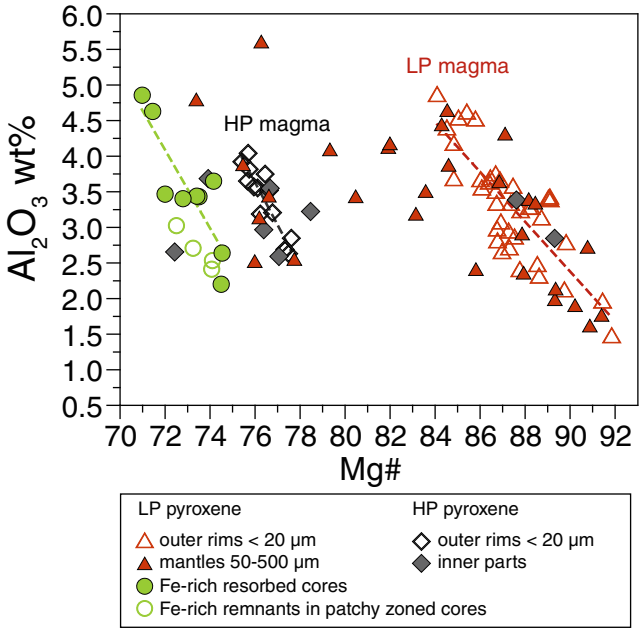

Fig. 6 Mg# [molar $100\times Mg/(Mg+Fe^{2+})$] versus $Al_2O_{3\ wt.\%}$ for clinopyroxenes of HP and LP products. Clinopyroxene composition defines three different trends of increasing Al_2O_3 contents with different Mg#s. High and intermediate Mg#s correspond, respectively, to crystallization from LP and HP magmas. Pyroxenes with lower Mg#s are supposed to be xenocrysts. *Symbols* are referred to different pyroxene types as discussed in the text and shown in Fig. 3

after experiencing different degrees of dissolution. Like olivine, clinopyroxene experienced episodes of growth under degassing conditions induced by the ascent of the LP magma. Some of these crystals remained in the magma system and subsequently acted as nuclei. Homogeneous and step-zoned mantles suggest that pyroxene also experience episodes of crystallization in equilibrium with the LP melt, possibly shifting the liquid phase towards more evolved compositions. Magmas with more evolved LP melts derived from the less evolved LP magmas through a process of crystallization, mainly of clinopyroxene Fs7–8, and likely represent the upper part of the LP magma column, where a comparatively lower volatile content forced the crystallization process. Crystallization and degassing were periodically interrupted by influx of new primitive magmas from depth.

Clinopyroxene Mg# 76–77 inherited from the HP magma show minor dissolution and thin rims <10 μm with less evolved compositions Mg#82–85 (Fs8–10) in equilibrium with the groundmass, suggesting slower crystallization/dissolution kinetics than plagioclase and olivine during the rapid ascent of the magma prior to eruption.

Eruption dynamics

The paroxysms that have occurred at Stromboli in past years consist of a sequence of explosive events usually lasting only a few minutes. They are characterized by cannon-like detonations and impulsive emissions of gas, ash and incandescent material which can rapidly evolve into kilometres-high convective plumes. The large-scale paroxysms are more complex sequences lasting up to a few hours and characterized, in addition, by a heavy rain of metre-sized incandescent clasts that cover the flanks of the volcano and in some cases trigger hot avalanches, as described in 1930 (Rittmann 1931). The seventeenth century paroxysm must have been a relatively short and complex eruption similar to that of 1930 as suggested by the characteristics and dispersal of the deposits (Bertagnini et al. submitted, Bull Volcanol). In particular, the occurrence of partially welded spatter deposits mantling the

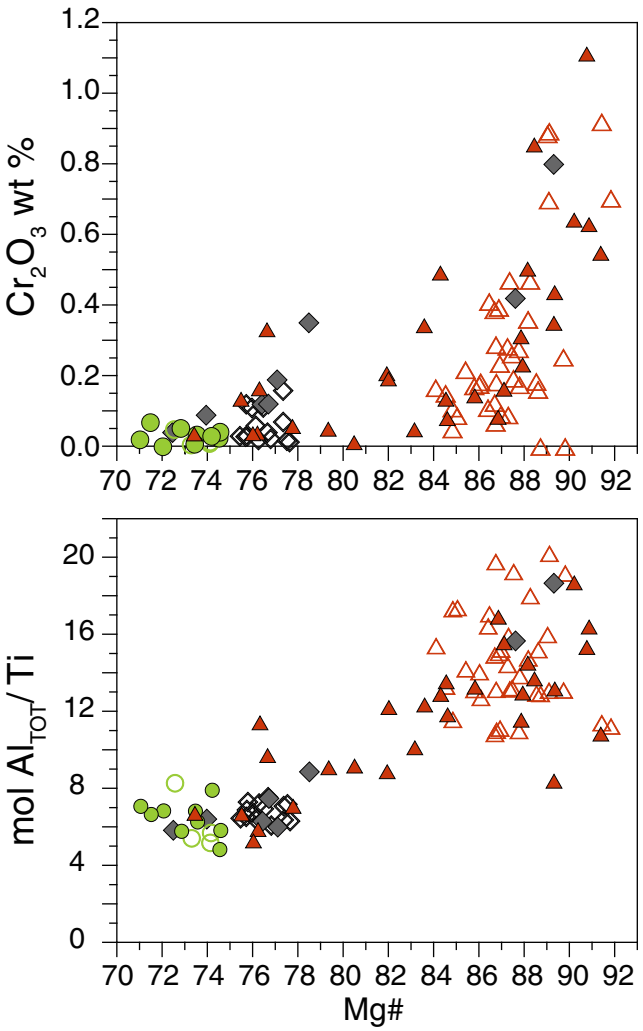

Fig. 7 Mg# [molar 100×Mg/(Mg+Fe^{2+})] versus Cr_2O_3wt.% and Al tot [^{IV}Al+^{VI}Al] /Ti molar ratio for clinopyroxenes of HP anl LP products. Positive correlations among Cr_2O_3, Al/Ti and Mg# are mainly induced by changes in melt composition from where clinopyroxene crystallized. *Symbols* are as in Fig. 6

flanks of Sciara del Fuoco several hundreds of metres away from the craters indicates moderate rates of accumulation of the hot and fluid pyroclasts on the ground and suggesting that a fire-fountain phase typical of Hawaiian style eruptions likely occurred during the eruption (Head and Wilson 1989; Sumner et al. 2005). Even Strombolian activity may be characterized by low, short-lived fountains which produce welded facies, but these are limited to tens of metres in lateral extent (Valentine and Gregg 2008).

During the early stages of the seventeenth century large-scale paroxysm, only a crystal-rich magma was erupted, except for minor quantities of LP magma during the opening phase. The HP magma emitted from Stromboli is a shallow, nearly completely degassed crystal mush (Métrich et al. 2001; Landi et al. 2004, 2008). It thus cannot produce energetic Strombolian explosions or fire-fountains without the involvement of an external volatile source. Volatile exsolution at depth from the LP magma and volatile accumulation at the top of the LP magma column could have generated a foam layer which became unstable and partly collapsed once a critical thickness was reached. At the beginning of the eruption, gas pockets might have entered the uppermost crystal-rich body and burst at shallow depths, likely as Strombolian explosions, producing ash and fine lapilli (layer 1 in Fig. 1). In this view, only minor quantities of magma from the top of the LP reservoir where the most evolved of the overall less-evolved LP magma resided, were dragged upwards during this phase. As degassing became more efficient, the buoyant bubble-rich magma column rose to the top and pushed the column of degassed crystal-rich magma up through the conduit, producing high intensity eruption, as already proposed for basaltic eruptions of variable style (Cimarelli et al. 2010; Sable et al. 2006). During this phase, only crystal-rich clasts were thrown over the flanks of the volcano (layer 2 and basal portion of the spatter (b) in Fig. 1). The upsection change from accumulation of flattened scoriae to welded layer indicates an increase in the magma discharge rate, likely forced by increasing acceleration of the melt and gas mixture upon decompression. During its rapid ascent, the LP magma mingled with the shallow degassed magma and finally erupted, giving rise to fountaining at the surface, which led to the deposition of the upper-part of the LP spatter. The absence of microlites in the sponge-like LP pyroclasts of the spatter indicates that decompression and magma ascent were fast enough to inhibit crystal nucleation.

The LP magma originates from the deeper part of the feeding system, possibly at a depth of between 7 and 11 km (Métrich et al. 2001, 2005, 2010; Bertagnini et al. 2003), so the magma dynamics during the opening phase of the eruption may have been strictly linked to CO_2 degassing. Based on mineral chemistry, repeated intrusions of primitive melts contributed to the evolution of the LP magma, and it is possible that an increase in the supply rate intensified CO_2 degassing at depth. Water exsolution at shallow depths likely played a dominant role in the later phases.

Alternative models have been proposed in the past years for the genesis of the sudden, short-lived paroxysmal explosions at Stromboli. Recent works by Aiuppa et al. (2009) and Allard (2010) suggest that the sudden coalescence and fast ascent of deep-derived CO_2-rich gas blobs is the main trigger and the driving force of paroxysms at Stromboli. In contrast, Métrich et al. (2001, 2005, 2010) and Bertagnini et al. (2003) suggest that paroxysms are triggered by the fast ascent of a foamy magma blob, with little or no gas–liquid decoupling required. The two interpretations, as a whole, refer to the two general models which have been adopted in the past to explain the origin of

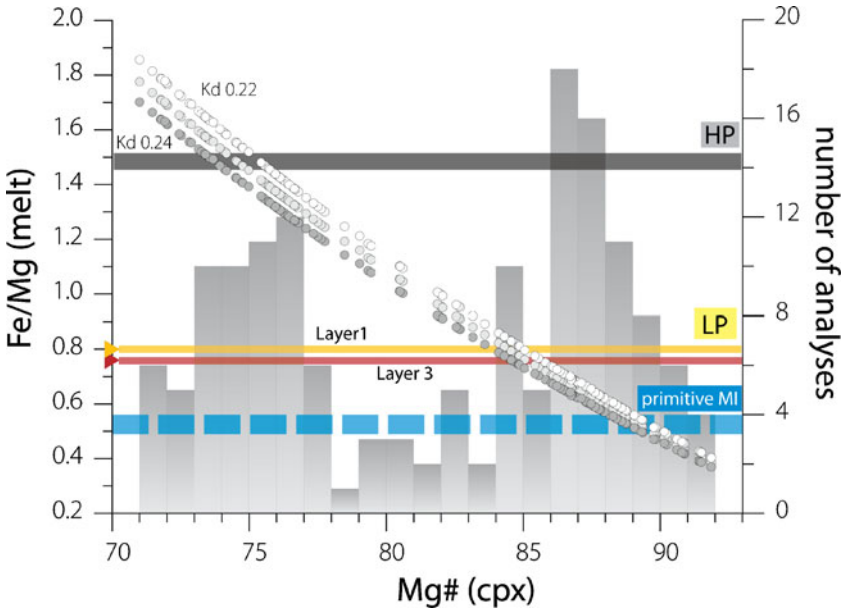

Fig. 8 Relationship between Fe/Mg (in moles) of matrix glasses and Mg# [molar 100× Mg/(Mg+Fe)] of clinopyroxene in HP and LP pyroclasts of the spatter. Histogram represents the clinopyroxene composition. *Circles* represent calculated Fe/Mg of melts in equilibrium with each clinopyroxene using $Kd^{cpx/liq}_{Fe-Mg}$ ranging from 0.22 to 0.24. All iron as Fe^{2+}. *Horizontal lines* indicate the average Fe/Mg of analyzed glasses. Representative Fe/Mg values of primitive MI hosted in olivine Fo88–90 from historical paroxysms are also reported (*dashed lines*; data from Bertagnini et al. 2003). See text for discussion

explosive basaltic eruptions: (1) a sudden collapse of a bubble foam layer (Vergniolle and Jaupart 1986; Jaupart and Vergniolle 1989) and (2) decompression and expansion of the gas during magma ascent producing homogeneous two-phase flow in which gas bubbles are "locked" to the magma (Parfitt and Wilson 1995; Parfitt 2004). We suggest that the sudden ascent of deeply derived CO_2-rich gas slugs triggered and drove the opening phase of the large-scale seventeenth century paroxysm. Rapid ascent and expansion of a foamy magma blob followed and was able to push out the overlying viscous magma and initiate and sustain a lava fountain.

Either an increase or decrease in release of CO_2-rich gas was measured before small-scale to intermediate paroxysms of recent years. This suggests that the mechanism that involves accumulation of CO_2 at depth followed by a sudden collapse of a bubble foam layer is consistent with only some paroxysmal explosions (Aiuppa et al. 2010). Lastly, the magnitude and eruptive dynamics of the paroxysms may depend on the extent to which CO_2 degassing at depth controls the process.

Summary and conclusions

Crystal-rich and crystal-poor (HP and LP) pyroclasts erupted during the seventeenth century, spatter-forming paroxysm have the texture and mineral composition typical of the HP and LP products erupted from Stromboli in recent decades. The LP magma reservoir involved in the eruption was compositionally zoned due to the crystallization of small quantities of clinopyroxene, mainly in its upper portion. Pyroxenes in equilibrium with the groundmass are only found in the external mantles of crystals grown on nuclei made up of either Fe-rich xenocrysts or sieve-textured, patchy-zoned crystals formed during episodes of destabilization and degassing in the LP reservoir. Evidence of disequilibrium is also observed in olivine. As a whole, the textural and mineral chemistry of the LP products records open system magmatic processes, such as repeated mafic recharge events and mixing with an older mushy body, as discussed by previous authors.

The base to top compositional and textural zoning of the deposit suggests that the eruption was triggered by the ascent of a deeply derived CO_2 gas slug, which was also responsible for the early explosive expulsion of the degassed HP magma together with minor quantity of LP magma from the top of the deep magma column. The magma dynamics then evolved into a homogeneous two-phase flow regime. The rapid ascent of the foamy magma blob pushed out the dense HP magma residing in the upper part of the reservoir and thus gave rise to moderate fountaining of LP magma and emplacement of a weakly agglutinated spatter far from the vent. Comparison between our results and dynamic models proposed for more recent paroxysms suggests that the magnitude and eruptive dynamics of the paroxysms are regulated by the interplay between CO_2 degassing at depth and rapid ascent of a vesiculated magma blob.

Acknowledgements This work has been supported by INGV-DPC programme. We are grateful to Jacopo Taddeucci for his careful review of the manuscript.

References

Allard P (2010) A CO_2-rich gas trigger of explosive paroxysms at Stromboli basaltic volcano, Italy. J Volcanol Geotherm Res 189:363–374

Aiuppa A, Federico C, Giudice G, Giuffrida G, Guida R, Gurrieri S, Liuzzo M, Moretti R, Papale P (2009) The 2007 eruption of Stromboli volcano: Insights from real-time measurements of the volcanic gas plume CO_2/SO_2 ratio. J Volcanol Geotherm Res 182:221–230. doi:10.1016/j.jvolgeores.2008.09.013

Aiuppa A, Burton M, Caltabiano T, Giudice G, Gurrieri S, Liuzzo M, Murè F, Salerno G (2010) Unusually large magmatic CO_2 gas emissions prior to a basaltic paroxysm. Geophys Res Lett 37: L17303. doi:10.1029/2010GL04383

Arrighi S, Rosi M, Tanguy JC, Courtillot V (2004) Recent eruptive history of Stromboli (Aeolian Islands, Italy) determined from high-accuracy archeomagnetic dating. Geophys Res Lett 31: L19603. doi:10.1029/2004GL020627

Barberi F, Rosi M, Sodi A (1993) Volcanic hazard assessment at Stromboli based on review of historical data. Acta Vulcanol 3:173–187

Bertagnini A, Coltelli M, Landi P, Pompilio M, Rosi M (1999) Violent explosions yield new insights into dynamics of Stromboli volcano. Eos Am Geoph Union Trans 80:633–636

Bertagnini A, Métrich N, Landi P, Rosi M (2003) Stromboli volcano (Aeolian Archipelago, Italy): An open window on the deep-feeding system of a steady state basaltic volcano. J Geophys Res 108(B7):2336. doi:10.1029/2002JB002146

Bertagnini A, Métrich N, Francalanci L et al (2008) Volcanology and magma geochemistry of the present-day activity: constraints on the feeding system. In: Calvari S, Inguaggiato S, Puglisi G, Ripepe M, Rosi M (eds) The Stromboli Volcano: An Integrated Study of the 2002–2003 Eruption. AGU, Washington, DC, pp 19–37. doi:10.1029/182GM04, AGU Geophysical Monograph Series 182

Cimarelli C, Di Traglia F, Taddeucci J (2010) Basaltic scoria textures from a zoned conduit as precursors to violent Strombolian activity. Geology 38:439–442. doi:10.1130/G30720.1

Conte AM, Perinelli C, Trigila R (2006) Cooling kinetics experiments on different Stromboli lavas: effects on crystal morphologies and phases composition. J Volcanol Geotherm Res 155:179–200

Di Carlo I, Pichavant M, Rotolo S, Scaillet B (2006) Experimental Crystallization of a High-K Arc Basalt: the Golden Pumice, Stromboli Volcano (Italy). J Petrol 47:1–27. doi:10.1093/petrology/egl011

Francalanci L, Tommasini S, Conticelli S (2004) The volcanic activity of Stromboli in the 1906–1998 period: mineralogical, geochemical and isotope data relevant to the understanding of Strombolian activity. J Volcanol Geotherm Res 131:179–211

Francalanci L, Davies GR, Lustenhouwer W, Tommasini S, Mason PRD, Conticelli S (2005) Intra-grain Sr isotope evidence for crystal recycling and multiple magma reservoirs in the recent activity of Stromboli volcano, Southern Italy. J Petrol 46:1997–2021. doi:10.1093/petrology/egi045

Ghiorso MS, Sack RO (1995) Chemical transfer in magmatic processes IV A revised and internally consistent thermodynamic model for the interpolation and extrapolation of liquid/solid equilibria in magmatic system at elevated temperatures and pressures. Contrib Mineral Petrol 119:197–212

Head JW, Wilson L (1989) Basaltic pyroclastic eruptions: influence of gas-release patterns and volume fluxes on fountain structure, and the formation of cinder cones, spatter cones, rootless flows, lava ponds and lava flows. J Volcanol Geotherm Res 37:261–271

Houghton BF, Wilson CJN (1989) A vesicularity index for pyroclastic deposits. Bull Volcanol 51:451–462

Jaupart C, Vergniolle S (1989) The generation and collapse of a foam layer at the roof of a basaltic magma chamber. J Fluid Mech 203:347–380

Landi P, Métrich N, Bertagnini A, Rosi M (2004) Dynamics of magma mixing and degassing recorded in plagioclase at Stromboli (Aeolian Archipelago, Italy). Contrib Mineral Petrol 147:213–227

Landi P, Francalanci L, Pompilio M, Rosi M, Corsaro RA, Petrone CM, Nardini I, Miraglia L (2006) The December 2002–July 2003 effusive event at Stromboli volcano, Italy: an insight into the shallow plumbing system by petrochemical studies. J Volcanol Geotherm Res 155:263–284

Landi P, Métrich N, Bertagnini A, Rosi M (2008) Recycling and "re-hydration" of degassed magma inducing transient dissolution/crystallization events at Stromboli (Italy). J Volcanol Geotherm Res 174:325–336

Marsella M, Coltelli M, Proietti C et al (2008) 2002–2003 Lava flow eruption of Stromboli: a contribution to understing lava discharge mechanisms using periodic digital photogrammetry survey. In: Calvari S, Inguaggiato S, Puglisi G, Ripepe M, Rosi M (eds) The Stromboli Volcano: An Integrated Study of the 2002–2003 Eruption. AGU, Washington, DC. doi:10.1029/182GM19, Geophysical Monograph Series 182

Métrich N, Bertagnini A, Landi P, Rosi M (2001) Crystallization driven by decompression and water loss at Stromboli volcano (Aeolian Islands, Italy). J Petrol 42:1471–1490

Métrich N, Bertagnini A, Landi P, Rosi M, Belhadj O (2005) Triggering mechanism at the origin of paroxysms at Stromboli (Aeolian Archipelago, Italy): the 5 April 2003 eruption. Geophys Res Lett 32:L10305. doi:10.1029/2004GL022257

Métrich N, Bertagnini A, Di Muro A (2010) Conditions of Magma Storage, Degassing and Ascent at Stromboli: New Insights into the Volcano Plumbing System with Inferences on the Eruptive Dynamics. J Petrol 51:603–626. doi:10.1093/petrology/egp083

Parfitt EA (2004) A discussion of the mechanisms of explosive basaltic eruptions. J Volcanol Geotherm Res 134:77–107

Parfitt EA, Wilson L (1995) Explosive volcanic eruptions: IX The transition between Hawaiian-style lava fountaining and Strombolian explosive activity. Geophys J Int 121:226–232

Pichavant M, Di Carlo I, Le Gac Y, Rotolo SG, Scaillet B (2009) Experimental constraints on the deep magma feeding system at Stromboli volcano, Italy. J Petrol 50:601–624. doi:10.1093/petrology/egp014

Pistolesi M, Rosi M, Pioli L et al (2008) The paroxysmal event and its deposits. In: Calvari S, Inguaggiato S, Puglisi G, Ripepe M, Rosi M (eds) The Stromboli Volcano: An Integrated Study of the 2002–2003 Eruption. AGU, Washington, DC, pp 317–329. doi:10.1029/182GM26, AGU Geophysical Monograph Series 182

Ripepe M, Delle Donne D, Harris AJL et al (2008) Dynamics of Strombolian Activity. In: Calvari S, Inguaggiato S, Puglisi G, Ripepe M, Rosi M (eds) The Stromboli Volcano: An Integrated Study of the 2002–2003 Eruption. AGU, Washington, DC. doi:10.1029/182GM05, AGU Geophysical Monograph Series 182

Rittmann A (1931) Der ausbruch des Stromboli am 11 September 1930. Z vulkanologie 14:47–7

Rosi M, Bertagnini A, Landi P (2000) Onset of the persistent activity at Stromboli volcano (Italy). Bull Volcanol 62:294–300

Rosi M, Bertagnini A, Harris AJL, Pioli L, Ripepe M (2006) A case history of paroxysmal explosion at Stromboli: timing and dynamics of the April 5, 2003 event. Earth Planet Sci Lett 243:594–606

Sable JE, Houghton BF, Del Carlo P, Coltelli M (2006) Changing conditions of magma ascent and fragmentation during the Etna 122 BC basaltic Plinian eruption: Evidence from clast microtextures. J Volcanol Geotherm Res 158:333–354

Speranza F, Pompilio M, Sagnotti L (2004) Paleomagnetism of spatter lavas from Stromboli volcano (Aeolian Islands, Italy): implica-

tions for the age of paroxysmal eruptions. Geophys Res Lett 31: L02607. doi:10.1029/20318944

Speranza F, Pompilio M, D'Ajello Caracciolo F, Sagnotti L (2008) Holocene eruptive history of the Stromboli volcano: constraints from paleomagnetic dating. J Geophys Res 113(B09101):1–23. doi:10.1029/2007JB005139

Streck M J (2008) Mineral textures and zoning as evidence for open system processes. In: Putirka KD and Tepley FJ III (eds) Rev Mineral Geochem 69:595–622

Sumner JM, Blake S, Matela RJ, Wolff JA (2005) Spatter. J Volcanol Geotherm Res 142:49–65

Tibaldi A (2001) Multiple sector collapses at Stromboli volcano, Italy: how they work. Bull Volcanol 63:112–125. doi:10.1007/s004450100129

Umino S, Horio A (1998) Multistage magma mixing revealed in phenocryst zoning of the Yunokuchi pumice, Akagi Volcano, Japan. J Petrol 39:101–124

Valentine GA, Gregg TKP (2008) Continental basalic volcanoes – Processes and problems. J Volcanol Geotherm Res 177:857–873

Vergniolle S, Jaupart C (1986) Separated two-phase flow and basaltic eruptions. J Geophys Res 91:12842–12860